Multimodal data analysis for Post-Decortication Therapy optimization using IoMT and Reinforcement Learning

Fahad Masood, Jawad Ahmad, Nada Alasbali, Ibtehal Nafea, Faisal Saeed, and Rahmat Ullah*

Abstract: Multimodal neural network approaches mirror clinical decision-making processes for therapy optimization. Multiple data sources, including images, Electronic Health Records (EHRs), and the Internet of Medical Things (IoMT), can be challenging for precise diagnoses. In this research, reinforcement learning, specifically Deep Q-Learning (DQL), utilizing multimodal data, has been employed to determine the most suitable treatment plans, particularly for patients undergoing lung decortication surgery. The model performance has been evaluated using rewards, epsilon decay, and Q-values across three different actions. The model's performance has also been compared with machine learning models, such as Naïve Bayes, K-Nearest Neighbor, Random Forest, Logistic Regression, and Support Vector Machine, regarding several performance metrics, including accuracy, precision, recall, and the area under the curve. Our findings demonstrate that the DQL model effectively learns optimal actions, significantly enhancing therapy optimization.

Keywords: Multimodal Data, Reinforcement Learning, Deep Q-Learning, IoMT, EHR

Fahad Masood, Department of Computing, Abasyn University Peshawar, 25000, Pakistan. email: fahad.masood@abasyn.edu.pk

Jawad Ahmad, Cybersecurity Center, Prince Mohammad Bin Fahd University, Alkhobar, 31952, Saudi Arabia. email: jahmad@pmu.edu.sa

Nada Alasbali, Department of Informatics and Computer Systems, College of Computer Science, King Khalid University, Abha 61421, Saudi Arbia. e-mail: Nalasbali@kku.edu.sa

Ibtehal Nafea, College of Computer Science and Engineering, Taibah University, Medina 41477, Saudi Arabia. email: inafea@taibahu.edu.sa

Faisal Saeed, College of Computing, Birmingham City University, Birmingham B4 7XG, UK. email: faisal.saeed@bcu.ac.uk

*Corresponding author: Rahmat Ullah, School of Computer Science and Electronic Engineering, University of Essex, Colchester CO4 3SQ, United Kingdom. email:rahmat.ullah@essex.ac.uk

1 Introduction

Decortication is a surgical procedure performed to remove the fibrous cortex, a thickened pleural layer around the lungs, which is often necessary for patients suffering from conditions such as chronic pleural effusion, empyema, or trapped lung. These pleural conditions typically arise from persistent inflammation, infections, or malignancy, causing the lungs to become restricted and impair normal respiratory function [1, 2]. The goal of decortication is to restore regular lung activity by removing the restrictive fibrous tissue, which in turn facilitates improved respiratory function. Post-surgery, patient recovery relies on a multidisciplinary approach, including respiratory therapy, pain management, and continuous monitoring to ensure rehabilitation success [3, 4].

Post-decorication therapy suffers a complex clinical decision-making challenge due to the heterogeneity of patient responses and the dynamic nature of post-surgical recovery. Effective personalization of treatment plans is crucial for reducing complications, enhancing outcomes, and improving patient quality of life. The latest convergence of Reinforcement Learning (RL), the Internet of Medical Things (IoMT), and multimodal health data presents an encouraging paradigm for automating and optimizing therapeutic decisions.

Multimodal data analysis has become an essential tool in the healthcare field in recent years, providing a holistic view of a patient's condition by integrating diverse data types such as medical imaging, clinical records, genetic information, and physiological measurements [5, 6]. This comprehensive approach enables personalized treatment planning and enhanced complication prediction, particularly in complex cases such as post-decortication recovery, where tailored therapeutic strategies can significantly impact patient outcomes [7].

The Internet of Medical Things (IoMT) further enhances post-surgical care by enabling the collection and analysis of real-time data from multiple sources, including imaging, electronic health records (EHRs), and genetic data [8]. By continuously monitoring patient conditions through IoMT-enabled devices, healthcare providers can receive real-time alerts when a patient's health status declines, ensuring timely interventions and minimizing the risk of complications [9, 10]. This real-time feedback loop facilitates more precise and effective post-decortication care.

Prior studies have explored various facets of this domain. For instance, Deep Learning (DL) algorithms have been applied to predict the risk of pancreatic cancer from disease trajectories. [11], while an enhanced DL technique has been developed for lung cancer classification [12]. Similarly, multimodal datasets, including imaging and lab tests, have been utilized for clinical diagnostics [13]. However, these works

often focus on a single modality, lack real-time adaptability, or do not explicitly consider personalized therapy paths post-decortication. Moreover, the integration of Deep Q- Learning (DQL) with real-time clinical indicators remains underexplored, especially in the context of IoMT-enhanced decision systems for thoracic surgery recovery.

To address these gaps, this study proposes a multimodal DQL-based framework that integrates IoMT data, X-ray images, and hematological markers to optimize treatment actions over time. The model is trained to maximize therapeutic reward by selecting the most appropriate intervention, monitoring, medication, or escalation based on the comprehensive patient state. The proposed system learns an optimal treatment plan by interacting with the multimodal environment and receiving rewards based on clinical improvements, enabling it to suggest the most effective action. This work contributes to the emerging field of intelligent healthcare by demonstrating the feasibility and effectiveness of a real-time, data-driven RL system tailored for post-surgical recovery management.

We apply DQL to multimodal data obtained from IoMT devices, EHRs, and medical imaging to develop personalized treatment plans for patients recovering from lung decortication surgery. By leveraging reinforcement learning, the model learns from real-time patient data to identify optimal therapeutic actions that can minimize complications and enhance recovery outcomes.

This study evaluates the performance of the DQL model across several key metrics, including reward signals, epsilon decay, and Q-values for different actions taken during the recovery process. The results are compared with traditional machine learning models, including Naïve Bayes, K-Nearest Neighbor, Random Forest, Logistic Regression, and Support Vector Machine. Performance is assessed using accuracy, precision, recall, and area under the curve (AUC) as metrics. Our findings demonstrate that the DQL model outperforms these traditional models in optimizing post-decortication care by effectively learning and implementing the most appropriate treatment actions.

The paper is structured as follows: Section 2 presents a comprehensive review of the relevant literature in machine learning and multimodal data analysis. Section 3 details the methodology employed in this study, including patient data collection, preprocessing, and the architecture of the reinforcement learning model. Section 4 discusses the model's implementation and performance, followed by a conclusion and future directions in Section 5.

2 Literature Review

Diagnostic accuracy, treatment procedures, and patient monitoring have been enhanced by the integration of multimodal AI in health care, which gave a transformative method for handling complex medical challenges in various medical domains, including radiology, oncology, dermatology, and cardiology [14][15][16][17]. Several Machine Learning (ML) and Deep Learning (DL) techniques, particularly Convolutional Neural Networks (CNN), Long Short Term Memory (LSTM), and Generative Adversarial Networks (GANs) have continuously pushed this field accelerative and enabled more enhanced analysis from both single and multimodal data [18, 19].

2.1 Background Study

A multimodal AI approach for the early detection of Alzheimer's disease has been investigated in recent years, combining various data types, including genetic information, neuroimaging, and clinical records [20]. Multimodal features, such as MRI/CT scan images and mild cognitive impairments, have been utilized in various machine learning techniques to offer significant performance in accurately predicting disease progression [21]. Time series data, biomarker discovery, and other novel approaches have delivered considerable results for predicting associated genes in the brain [22] [23] [24].

Electronic health records (EHRs), patient reports, and clinical notes are critical in predicting and analyzing depression in patients. AI models play a crucial role in identifying patterns and relationships for effective and personalized treatment procedures. Kalmady et al. utilized transfer learning with depression prediction, while anxiety disorders were also reported using clinical and MRI data [25]. Rehospitalization prediction for depression patients, identification of bipolar disorders, and Alcohol effect prediction have been performed using multimodal data [26] [27] [28].

AI-enabled multimodal approaches were pivotal for assessing disease severity through MRI, CT Scan, and X-ray images, especially during the COVID-19 pandemic [29, 30]. The images were integrated with the patient's clinical and health records to facilitate quick responses to health decisions. An IoT-based framework using multimodal data was presented for the effective detection of COVID-19, while ML models were used with the multimodal data for an enhanced detection framework [31].

Mammograms and CT scan images, combined with multimodal data, enhanced the diagnostic precision for breast and lung cancers. The complex image features

were analyzed using DL algorithms and correlated with the genetic markers for the identification of cancer types [32] [33]. The enhancement supported precise prognosis and treatment plans for cancer patients [34]. Various cancer diseases have been identified and treated through comprehensive studies using multimodal data with deep learning [35, 36].

Multimodal data analysis in healthcare has revolutionized the detection, treatment, and monitoring of various diseases, providing comprehensive insights. It has provided a broad path for the healthcare sector in detecting various diseases, ranging from cancer to brain disorders, Alzheimer's, and other conditions. The synergy of genetic, image, and clinical data has established critical perspectives in improving the effectiveness of diagnoses and is further transforming the landscape of the health sector.

2.2 Research Gap and Comparative Analysis

While several studies have explored features of clinical decision support using machine learning or deep learning methods, the proposed approach addresses various critical research gaps that have not been effectively covered in the literature. Existing studies focus on multimodal data sources, which may overlook meaningful interactions between physiological, biochemical, and imaging features. The current study integrates X-ray images, laboratory results, and real time IoMT sensor data into a cohesive model that enables more informed and personalized therapy optimization.

Supervised learning models, including support vector machines (SVM), decision trees, or random forests, have been used in previous studies for diagnostic or prognostic tasks. These models' shortfalls are the lack of capacity to learn treatment strategies over time adaptively. In this work, a deep Q-learning framework is employed, enabling dynamic and sequential decision-making based on patient state transitions and therapy outcomes. Real-time IoMT data streams into therapeutic decisions, bridging the gap in the decision-making process. The reward-based framework evaluates the immediate and cumulative effects of various treatment actions, enabling more responsive and patient-specific care. The action-reward cycle enables the system to refine its treatment strategy based on observed patient responses continually. '
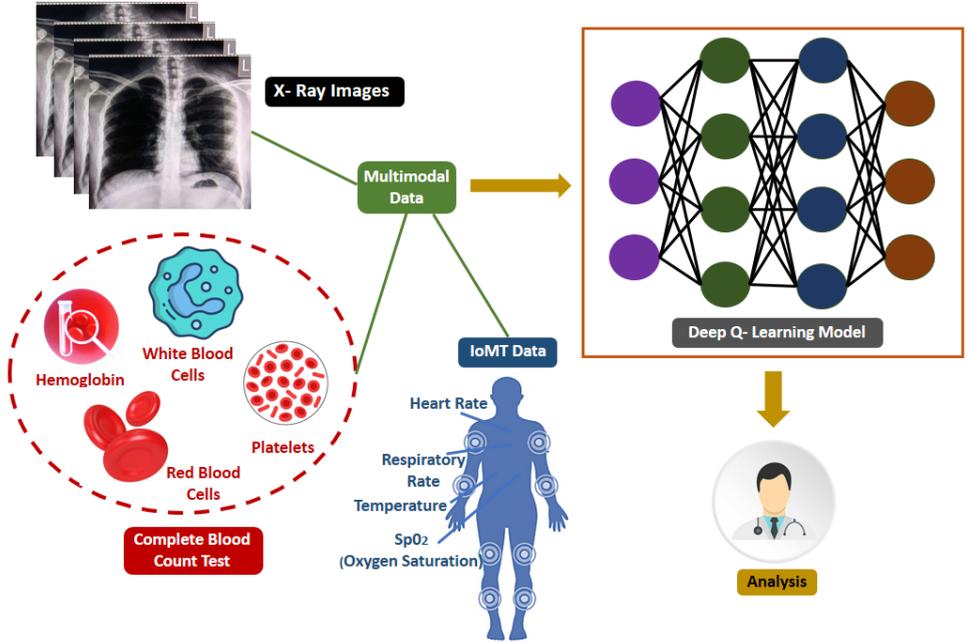
Fig. 1: The proposed framework architecture. This diagram illustrates the process of combining X-ray images and comprehensive blood test results with real-time IoMT data, such as heart rate, respiratory rate, and oxygen saturation, to inform a Deep Q-learning model. Source: Created by the authors

3 Methodology

This research aims to optimize post-decortication therapy by employing the Deep Q-Learning (DQL) model, a reinforcement learning approach. The framework utilizes multimodal data, including medical imaging, Electronic Health Records (EHRs), and patient monitoring data, as shown in Figure 1. The first phase is data collection from the patients who have undergone decortication surgery. In the next phase, data preprocessing is performed to obtain numerical data from the X-ray images for integration with the other modalities. The diverse dataset is then analyzed by training the DQL model. The patient data have been fed into the model to learn the optimal schemes used for post-decortication therapy. The model was validated during the testing phase to evaluate its effectiveness, thus refining the therapeutic endorsements accordingly. A detailed description of the proposed framework is presented in this section.

3.1 Data Collection

Data collection has been performed for 1250 patients, both male and female, who underwent decortication surgery. Patients were referred for 48 hours to collect data, including X-ray images, Electronic Health Records (EHRs), and Internet of Medical Things (IoMT). The data provided includes information on lung conditions, blood test reports, and continuous patient monitoring from wearable devices equipped with sensors. The dataset description is detailed in the Data Availability section.

3.1.1 Data extraction using X-ray Images

The structural and post-surgical lung conditions were analyzed by extracting numerical data from high-resolution X-ray images in JPEG and DICOM formats. Image preprocessing is then performed by standardizing pixel values, resizing, and minimizing noise to obtain image clarity. The vital areas, including fibrous tissue, have been identified using segmentation and quantitative analysis for various feature calculations. The feature details are outlined in Table 1.

Sr. No	Parameter	Normal Value	Abnormal Value
1	Lung Volume and Expansion	70-90%	<70% or >90%
2	Pleural Thickness	< 2-3 mm	> 3 mm
3	Opacity Quantification	-800 to -1000	outside (-800 to -1000)
4	Air and Fluid Levels	100-200 mL	> 200 mL
5	Diaphragm Position and Motion	< 2-3 cm	> 3 cm
6	Rib Cage Metrics	< 1-2 cm	> 2 cm
7	Quantification of Atelectasis	< 1-2 cm^2	> 2 cm^2

Tab. 1: Parameter details from X-ray images.

3.1.2 Electronic Health Record

Electronic Health Records (EHRs) were collected for all patients, including medical history, demographic data, and treatment procedures. Several critical parameters, including Hemoglobin (Hb), Hematocrit (Hct), Red Blood Cell Count (RBC), White Blood Cell Count (WBC), and Platelet Count, were obtained and analyzed from Complete Blood Count (CBC) tests. The complete details of the parameters included in the CBC test have been shown in Table 2.

No	Parameter	Normal Value	Abnormal Value
1	Hemoglobin (Hb)	Men: 13.8-17.2 g/dL Women: 12.1-15.1 g/dL	< 12.0 g/dL (low) or > 17.2 g/dL (high)
2	Hematocrit (Hct)	Men: 40.7%-50.3% Women: 36.1%-44.3%	< 36.1% (low) or > 50.3% (high)
3	Red Blood Cell Count (RBC)	Men: 4.7-6.1 million/μL Women: 4.2-5.4 million/μL	<4.2 mil/μL (low) or > 6.1 mil/μL (high)
4	White Blood Cell Count (WBC)	4.0-11.0x 10^9/L	< 4.0 x 10^9/L (low) or > 11.0 x 10^9/L (high)
5	Platelet Count	150 -450 x 10^9/L	<150 x 10^9/L (low) or >450 x 10^9/L (high)
6	Mean Corpuscular Volume (MCV)	80-100 fL	< 80 fL (low) or > 100 fL (high)
7	Mean Corpuscular Hemoglobin (MCH)	27 - 31 pg/cell	< 27 pg/cell (low) or > 31 pg/cell (high)
8	Mean Corpuscular Hemoglobin Concentration	33.4 - 35.5 g/dL	< 33.4 g/dL (low) or > 35.5 g/dL (high)
9	Red Cell Distribution Width	11.5% - 14.5%	< 11.5% (low) or > 14.5% (high)

Tab. 2: Electronic Health Record details for various parameters.

3.1.3 IoMT Data

The Internet of Medical Things (IoMT) network collected real-time patient data using different sensors. The IoMT parameters were monitored, including heart rate, temperature, respiratory rate, SpO2 (Oxygen Saturation), and glucose level. The details of the parameters have been discussed in Table 3.

Sr. No	Parameter	Normal Value	Abnormal Value
1	Heart Rate	60 - 100 beats/ min	< 60 or > 100 beats/min
2	Respiratory Rate	12 - 20 breaths/min	< 12 or > 20 breaths/min
3	Temperature	36.1 - 37.2°C (97 - 99°F)	< 36.1°C or > 37.2°C
4	Glucose Levels	70 - 100 mg/dL (fasting)	< 70 or > 100 mg/dL (fasting)
5	SpO$_2$ (O$_2$ Saturation)	95% - 100%	< 95%

Tab. 3: Real-time patient monitoring features.

3.2 Deep Q- Learning Framework

Deep Q-learning (DQL) handles large state-action spaces by employing a Reinforcement Learning (RL) approach that combines Q-learning with neural networks. DQL supports post-decortication therapy optimization by utilizing multimodal patient data to enhance patient recovery and prolong its impacts. This section presents the detailed framework description.

3.2.1 Markov Decision Process

The Markov decision process in the DQL framework comprises agents, states, actions, and reward functions that determine the optimal plan based on the patient's health condition. The state s_t at the given time 't' represents the patient's health record obtained from X-ray images (X_t), EHR (E_t), and IoMT (I_t) data. Mathematically s_t can be denoted as $s_t = [X_t, E_t, I_t]$. The RL agent selects possible mediations of different actions a_t from the given action space based on s_t. The state and actions are mapped and guided by an optimal policy to improve the predicted reward. The outcome of the immediate treatment procedure is represented by a reward r_t, which may be positive or negative depending on the patient's condition. If the patient's health improves, the reward for the action taken will be positive; otherwise, it will be negative. The state change from s_t to s'_t after applying a_t is referred to as the state transition. It represents the patients' updated condition based on the selected treatment plan.

3.2.2 Q-Function and Q-Learning

The Q-function utilizes the Bellman equation by acting a_t in state s_t at the given time 't' and is updated mathematically as,

$$Q(s_t, a_t) = Q(s_t, a_t) + \alpha \left(r_t + \gamma \max_{a'} Q(s_{t+1}, a') - Q(s_t, a_t) \right) \tag{1}$$

where α is the learning rate, γ is the discount factor, r_t is the immediate reward, and s_{t+1} is the next state after action a_t. The deep neural network (Q-network) in DQL is utilized due to the large state space, i.e., multimodal patient data, to estimate the Q-function. The Q- network $Q(s, a : \theta)$ obtains patient state s_t and returns Q- values for each a_t where θ represents the network parameter. The

Q-network is trained using the loss function expressed as,

$$L(\theta) = E\left[y_t - Q(s_t, a_t; \theta)\right] \tag{2}$$

where y_t is the target represented as,

$$y(t) = r_t + \gamma \max_{a'} Q\left(s_{t+1}, a' : \theta^-\right) \tag{3}$$

The learning stability in the Q-network during training is improved by storing (s_t, a_t, r_t, s_{t+1}) in a replay buffer, thereby reducing the correlations between samples. The ϵ- greedy policy is followed for new treatments, and the treatments with high rewards to highlight the exploration and exploitation. When the probability is ϵ, the new treatment plans are explored, and for $1 - \epsilon$, the treatment with the highest Q-values is exploited using random actions. The learned Q-function is maximized to improve the policy by selecting the optimal action a_t in state s_t for therapy. The updated policy can be represented as,

$$s_t = arg \max_{a_t} Q\left(s_t, a_t : \theta\right) \tag{4}$$

The complete algorithm description is given in Algorithm 1.

4 Analysis and Discussion

This section provides an overview of the experimental outcomes and analysis conducted to evaluate the performance of the proposed reinforcement learning-based model. The focus is on describing the methodological setup and the performance metrics to assess the model's effectiveness. The detailed numerical results and the critical analysis are presented in the following sections.

4.1 Simulation Setup

In this section, the simulation environment developed to assess the performance of the proposed decision-making framework is presented using deep learning. The Intel Core i7-1165G7 CPU was used in conjunction with 16GB of DDR4 memory and Intel Iris Xe graphics to run the model. The Q values were initialized in the range [0.5, 0.1] to reflect an optimistic initial estimate conducive to faster convergence. A total of 100 episodes were conducted to average the results and to allow sufficient learning.

Algorithm 1 DQL algorithm for the proposed therapy optimization

---

1: **Initialize:**
2: Initialize Q-network $Q(s, a; \theta)$ with random weights θ.
3: Initialize target Q-network $\hat{Q}(s, a; \theta^-)$ with weights $\theta^- = \theta$.
4: Initialize replay memory $\mathcal{D}$ with capacity $D_{\max}$.
5: Set learning rate α, discount factor γ, and exploration rate ϵ.
6: **for** each episode $i = 1$ to N **do**
7:     Initialize state s_0 from patient data (e.g., X-ray, EHR, IoMT).
8:     **for** each time step t **do**
9:         **Action Selection:**
10:         **if** Random number $< \epsilon$ **then**
11:             Select random action a_t (exploration).
12:         **else**
13:             Select action $a_t = \arg\max_a Q(s_t, a; \theta)$ (exploitation).
14:         **end if**
15:         **Execute Action:** Apply selected action a_t.
16:         Observe reward r_t and next state s_{t+1}.
17:         Store experience (s_t, a_t, r_t, s_{t+1}) in replay memory $\mathcal{D}$.
18:         **Replay Sampling:** Sample a minibatch from $\mathcal{D}$.
19:         **for** each sampled experience (s_j, a_j, r_j, s_{j+1}) **do**
20:             **Q-value Update:**
21:             **if** s_{j+1} is terminal **then**
22:                 $y_j = r_j$.
23:             **else**
24:                 $y_j = r_j + \gamma \max_{a'} \hat{Q}(s_{j+1}, a'; \theta^-)$.
25:             **end if**
26:             Update Q-network by minimizing loss $L(\theta) = \frac{1}{M} \sum_j \left(y_j - Q(s_j, a_j; \theta) \right)^2$.
27:         **end for**
28:         Periodically update target network $\theta^- = \theta$ (every C steps).
29:     **end for**
30:     Decay exploration rate ϵ for reduced exploration over time.
31: **end for**

4.2 Results Analysis

The deep Q-learning model relies on epsilon decay values for an exploration-exploitation balance during training. It begins with an initial value of 0.95, which enables the model to evaluate various treatment schemes involving X-ray, EHR, and IoMT data, as illustrated in Figure 2. Each action provides a prospective outcome for a wide range of experiences. The epsilon value is minimized to 0.01, showing a deliberate shift from exploration to exploitation. It enables the agent to make more conversant treatment choices based on acquired knowledge and Q-values. The effective implementation of the epsilon-greedy strategy is beneficial for optimizing therapy in all three actions.
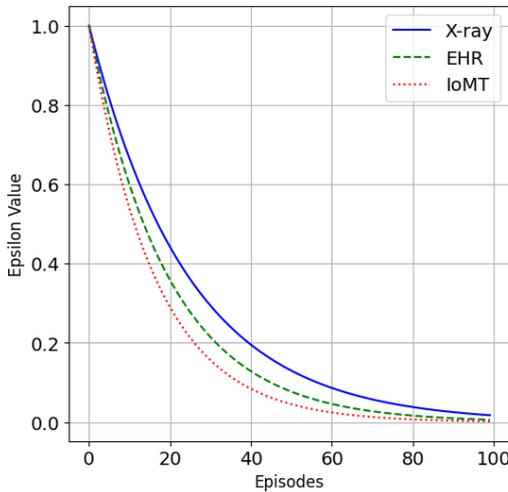
Fig. 2: Epsilon decay for mean 100 episodes from X-ray, EHR, and IoMT data. Source: Created by the authors.

Figures 3 and 4 show the Q-values and reward optimization for all three actions across episodes. Action 1 focuses on treatment centered on X-ray data, while Action 2 corresponds to Electronic Health Records (EHR) data, and Action 3 associates with IoMT data. It is worth noting that the model's progress in learning is promising, with lower rewards in the initial episodes and a steadily increasing trend as the episodes progress. The balance between exploration and exploitation also shows the model's ability to learn better action-taking policies that improve the reward.

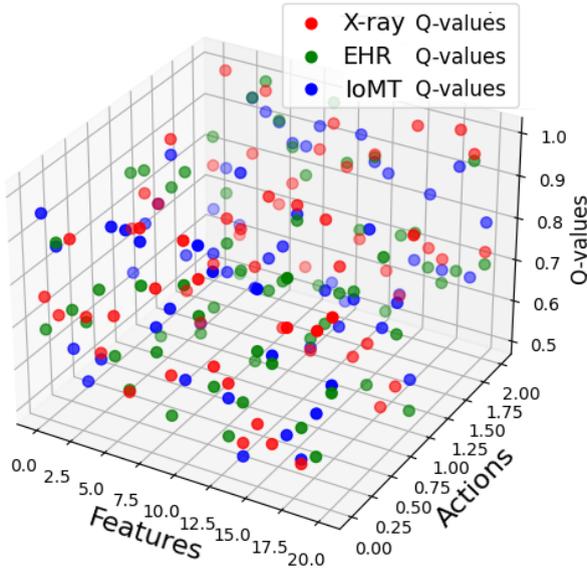Figure 5 shows the comparative results of the model performance in terms

Fig. 3: 3D Q values for all the actions from X-ray, EHR, and IoMT data. Source: Created by the authors

of accuracy with the machine learning models, including KNN, SVM, RF, NB, and SVM. It is noticeable that the DQL model yields better results in correctly predicting actions for therapy optimization.

The statistical results for both the Q-values and rewards are shown in Figures 6(a) and 6(b), providing a profound understanding of learning scenarios for all three actions. It has been indicated that actions related to the X-ray image data attained the highest median reward, while the other actions for EHR and IoMT data were nearly equal. The action performed for the IoMT data in terms of Q-values is the highest among the other actions. The overall results indicate that the model has been successful in optimizing therapy through the analysis of multimodal data.

4.3 Critical Evaluation

A comprehensive sensitivity analysis has been performed to extract clinically relevant insights and evaluate the robustness of the proposed framework. The key findings reveal that respiratory indicators, including SPO2, respiratory rate, and lung volume, exert the greatest influence on both action selection and cumulative reward. These features consistently altered the trajectory of the learned policy,
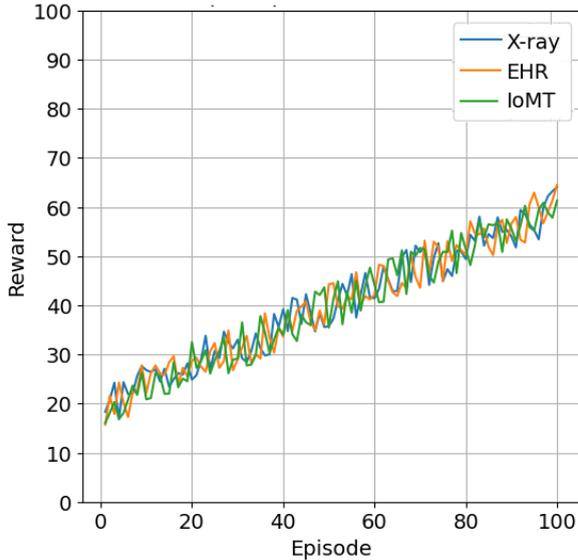
Fig. 4: Reward values of mean 100 episodes for all the actions from X-ray, EHR, and IoMT data. Source: Created by the authors
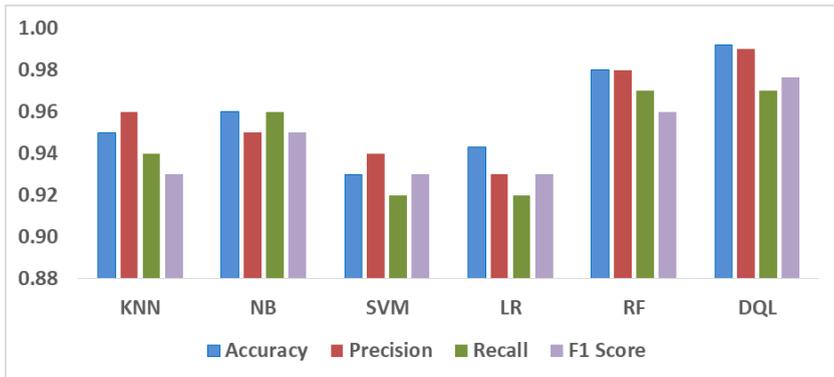

Fig. 5: Comparison results of the proposed DQL model with the machine learning models. Source: Created by the authors

underscoring their critical role in optimizing post-decortication therapy. Adjusting the reward threshold demonstrates a clear trade-off, while more conservative thresholds yielded fewer immediate positive rewards. It promotes long-term policy stability and improved outcomes. It suggests that fine-tuning the reward definition is essential for aligning agent behaviour with clinical risk aversion.
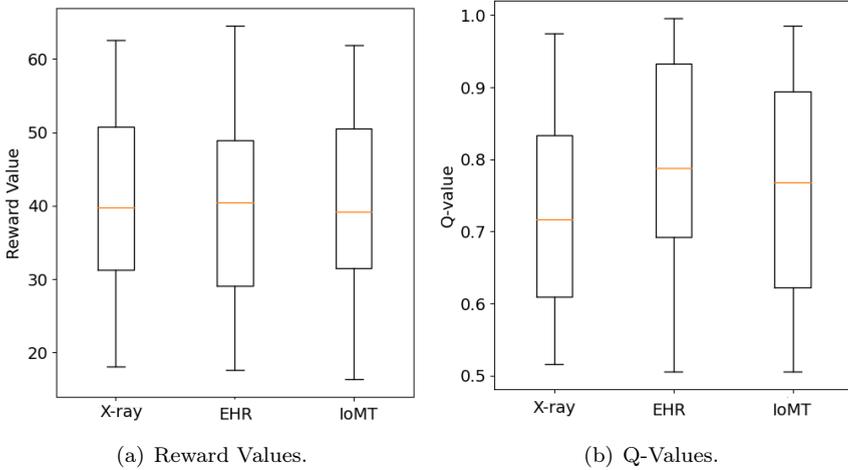
(a) Reward Values.

(b) Q-Values.

Fig. 6: Statistical results of the proposed DQL model for X-ray, EHR, and IoMT data. Source: Created by the authors

The epsilon decay modification rate showed that overly aggressive decay led to premature convergence and limited exploration On the other hand, a more gradual decay ensured sufficient exploration in early episodes and facilitated improved convergence to optimal actions. Moreover, the agent's performance remained stable when exposed to simulated noise in IoMT sensor data, including fluctuations in sugar levels and heart rates. It shows that the framework is robust to typical real-world variability in sensor-driven health monitoring environments. These observations exhibit that the proposed model is not only sensitive to clinically relevant features but also reveals resilience to variations in system parameters and sensor inputs, which makes it suitable for the post-surgical therapy optimization.

5 Conclusion

Reinforcement learning strategies, particularly Deep Q-Learning (DQL), are crucial tools for optimizing therapy research in healthcare. Multimodal data sources, combined with the DQL model, can facilitate precise clinical decision-making for effective treatment. In this study, multimodal data analysis has been performed for therapy optimization related to post-decortication surgery. Data sources, including X-ray images, patients' electronic health records, and medical information, have been utilized to determine optimal action plans and treatment procedures. This

conclusion conveys a new indication for the benefit of multimodal data in medical applications. It is noteworthy that DQL-based multimodal data analysis is a more effective choice for utilizing multiple modalities in therapy optimization. Although X-ray images have been used in the present study, we plan to extend this effort by including CT scans and MRI images in the future.

Author contributions

F. M. was responsible for the manuscript writing, research framework design, and model creation, and data analysis. J.A. was responsible for coding and liaising as part of the research project, organizing research data, proofreading language, and processing images. N. A. was responsible for mode creation and data analysis. I. N. was responsible for organizing the research data, proofreading the language, and data analysis. F. S. was responsible for model creation, data analysis, and proofreading. All authors have read and agreed to the published version of the manuscript

Conflict of interest

The authors declare no conflict of interest regarding the publication of this article.

Data availability statement

The images and electronic health records cannot be shared due to ethical limits, as they contain the patient's biographical information. The university ethics committee did not permit sharing the sensitive data publicly. However, only the IoMT dataset can be accessed through the given repository link https://github.com/researchcsaup/PostDecortication/blob/a6b287972da7a7c8ea36cd0a92f2b858e32c1e14/IoMT_Data.csv.

References

[1] Rappaport, J. M., Siddiqui, H. U., Tang, A., Thuita, L. W., Raja, S., Bribriesco, A., ... & Ahmad, U. (2021). Pleural space management after lung transplant: Early and late outcomes of pleural decortication. The Journal of Heart and Lung Transplantation, 40(7), 623-630. DOI

[2] Bolourani, S., Wang, P., Patel, V. M., Manetta, F., & Lee, P. C. (2020). Predicting respiratory failure after pulmonary lobectomy using machine learning techniques. Surgery, 168(4), 743-752. DOI

[3] Zorbas, K. A., Abbas, A. E. S., Song, K. J., Zorbas, I. A., Lois, W., & Burack, J. H. (2023). A simple prediction score for postoperative mortality after decortication. Journal of Thoracic Disease, 15(12), 6483. DOI

[4] Liu, X., Wang, X., Sheng, J., Jiang, Y., Li, L., & Dai, X. (2023). Open decortication for patients presenting with stage III tuberculous empyema with low density lines on CT imaging. Scientific Reports, 13(1), 9658.DOI

[5] Shaik, T., Tao, X., Li, L., Xie, H., & Velásquez, J. D. (2024). A survey of multimodal information fusion for smart healthcare: Mapping the journey from data to wisdom. Information Fusion, 102, 102040. DOI

[6] Cremonesi, F., Planat, V., Kalokyri, V., Kondylakis, H., Sanavia, T., Resinas, V. M. M., ... & Uribe, S. (2023). The need for multimodal health data modeling: A practical approach for a federated-learning healthcare platform. Journal of Biomedical Informatics, 141, 104338. DOI

[7] Yildirim, N., Richardson, H., Wetscherek, M. T., Bajwa, J., Jacob, J., Pinnock, M. A., ... & Thieme, A. (2024, May). Multimodal healthcare AI: identifying and designing clinically relevant vision-language applications for radiology. In Proceedings of the CHI Conference on Human Factors in Computing Systems (pp. 1-22).DOI

[8] Ahmed, S. F., Alam, M. S. B., Afrin, S., Rafa, S. J., Rafa, N., & Gandomi, A. H. (2024). Insights into Internet of Medical Things (IoMT): Data fusion, security issues and potential solutions. Information Fusion, 102, 102060. DOI

[9] Ding, X., Zhang, Y., Li, J., Mao, B., Guo, Y., & Li, G. (2023). A feasibility study of multi-mode intelligent fusion medical data transmission technology of industrial Internet of Things combined with medical Internet of Things. Internet of Things, 21, 100689. DOI

[10] Wornow, M., Xu, Y., Thapa, R., Patel, B., Steinberg, E., Fleming, S., ... & Shah, N. H. (2023). The shaky foundations of large language models and foundation models for electronic health records. npj Digital Medicine, 6(1), 135. DOI

[11] Placido, D., Yuan, B., Hjaltelin, J.X., Zheng, C., Haue, A.D., Chmura, P.J., Yuan, C., Kim, J., Umeton, R., Antell, G. and Chowdhury, A., 2023. A deep learning algorithm to predict risk of pancreatic cancer from disease trajectories. Nature medicine, 29(5), pp.1113-1122. DOI

[12] Sangeetha, S.K.B., Mathivanan, S.K., Karthikeyan, P., Rajadurai, H., Shivahare, B.D., Mallik, S. and Qin, H., 2024. An enhanced multimodal fusion deep learning neural network for lung cancer classification. Systems and Soft Computing, 6, p.200068. DOI

[13] Huang, S.C., Huo, Z., Steinberg, E., Chiang, C.C., Langlotz, C., Lungren, M., Yeung, S., Shah, N. and Fries, J., 2023. INSPECT: a multimodal dataset for patient outcome prediction of pulmonary embolisms. Advances in Neural Information Processing Systems, 36, pp.17742-17772. Link

[14] Heiliger, L., Sekuboyina, A., Menze, B., Egger, J., & Kleesiek, J. (2022). Beyond medical imaging-a review of multimodal deep learning in radiology. TechRxiv, (19103432). DOI

[15] Steyaert, S., Pizurica, M., Nagaraj, D., Khandelwal, P., Hernandez-Boussard, T., Gentles, A. J., & Gevaert, O. (2023). Multimodal data fusion for cancer biomarker discovery with deep learning. Nature machine intelligence, 5(4), 351-362. DOI

[16] Yap, J., Yolland, W., & Tschandl, P. (2018). Multimodal skin lesion classification using deep learning. Experimental dermatology, 27(11), 1261-1267. DOI

[17] Hernandez, L., Kim, R., Tokcan, N., Derksen, H., Biesterveld, B. E., Croteau, A., ... & Gryak, J. (2021). Multimodal tensor-based method for integrative and continuous patient monitoring during postoperative cardiac care. Artificial Intelligence in Medicine, 113, 102032.

[17] Hernandez, L., Kim, R., Tokcan, N., Derksen, H., Biesterveld, B. E., Croteau, A., ... & Gryak, J. (2021). Multimodal tensor-based method for integrative and continuous patient monitoring during postoperative cardiac care. Artificial Intelligence in Medicine, 113, 102032. DOI

[18] Masood, F., Khan, W. U., Ullah, K., Khan, A., Alghamedy, F. H., & Aljuaid, H. (2023). A hybrid CNN-LSTM random forest model for dysgraphia classification from hand-written characters with uniform/normal distribution. Applied Sciences, 13(7), 4275. DOI

[19] Aftab, N., Masood, F., Ahmad, S., Rahim, S. S., Sanami, S., Shaker, B., & Wei, D. Q. (2024). An Optimized Deep Learning Approach for Blood-Brain Barrier Permeability Prediction with ODE Integration. Informatics in Medicine Unlocked, 101526. DOI

[20] Bi, X. A., Hu, X., Xie, Y., & Wu, H. (2021). A novel CERNNE approach for predicting Parkinson's Disease-associated genes and brain regions based on multimodal imaging genetics data. Medical Image Analysis, 67, 101830. DOI

[21] Yang, L., Wang, X., Guo, Q., Gladstein, S., Wooten, D., Li, T., ... & Alzheimer's Disease Neuroimaging Initiative. (2021). Deep learning based multimodal progression modeling for Alzheimer's disease. Statistics in Biopharmaceutical Research, 13(3), 337-343. DOI

[22] Lin, W., Gao, Q., Yuan, J., Chen, Z., Feng, C., Chen, W., ... & Tong, T. (2020). Predicting Alzheimer's disease conversion from mild cognitive impairment using an extreme learning machine-based grading method with multimodal data. Frontiers in aging neuroscience, 12, 77. DOI

[23] El-Sappagh, S., Abuhmed, T., Islam, S. R., & Kwak, K. S. (2020). Multimodal multitask deep learning model for Alzheimer's disease progression detection based on time series data. Neurocomputing, 412, 197-215. DOI

[24] Venugopalan, J., Tong, L., Hassanzadeh, H. R., & Wang, M. D. (2021). Multimodal deep learning models for early detection of Alzheimer's disease stage. Scientific reports, 11(1), 3254. DOI

[25] Kalmady, S. V., Paul, A. K., Narayanaswamy, J. C., Agrawal, R., Shivakumar, V., Greenshaw, A. J., ... & Reddy, Y. J. (2022). Prediction of obsessive-compulsive disorder: importance of neurobiology-aided feature design and cross-diagnosis transfer learning. Biological Psychiatry: Cognitive Neuroscience and Neuroimaging, 7(7), 735-746. DOI

[26] Hilbert, K., Lueken, U., Muehlhan, M., & Beesdo-Baum, K. (2017). Separating generalized anxiety disorder from major depression using clinical, hormonal, and structural MRI data: A multimodal machine learning study. Brain and behavior, 7(3), e00633. DOI

[27] Kinreich, S., Meyers, J. L., Maron-Katz, A., Kamarajan, C., Pandey, A. K., Chorlian, D. B., ... & Porjesz, B. (2021). Predicting risk for Alcohol Use Disorder using longitudinal data with multimodal biomarkers and family history: a machine learning study. Molecular psychiatry, 26(4), 1133-1141. DOI

[28] Ceccarelli, F., & Mahmoud, M. (2022). Multimodal temporal machine learning for Bipolar Disorder and Depression Recognition. Pattern Analysis and Applications, 25(3), 493-504. DOI

[29] Jayachitra, V. P., Nivetha, S., Nivetha, R., & Harini, R. (2021). A cognitive IoT-based framework for effective diagnosis of COVID-19 using multimodal data. Biomedical Signal Processing and Control, 70, 102960. DOI

[30] Umair, M., Khan, M.S., Ahmed, F., Baothman, F., Alqahtani, F., Alian, M., & Ahmad, J. (2021). Detection of COVID-19 Using Transfer Learning and Grad-CAM Visualization on Indigenously Collected X-ray Dataset. Sensors, 21, 5813. DOI

[31] Zeng, W., Gautam, A., & Huson, D. H. (2021). On the application of advanced machine learning methods to analyze enhanced, multimodal data from persons infected with COVID-19. Computation, 9(1), 4. DOI

[32] Sun, D., Wang, M., & Li, A. (2018). A multimodal deep neural network for human breast cancer prognosis prediction by integrating multi-dimensional data. IEEE/ACM transactions on computational biology and bioinformatics, 16(3), 841-850. DOI

[33] Yan, R., Ren, F., Rao, X., Shi, B., Xiang, T., Zhang, L., ... & Zhang, F. (2019). Integration of multimodal data for breast cancer classification using a hybrid deep learning method. In Intelligent Computing Theories and Application: 15th International Conference, ICIC 2019, Nanchang, China, August 3–6, 2019, Proceedings, Part I 15 (pp. 460-469). Springer International Publishing. DOI

[34] Tang, X., Xu, X., Han, Z., Bai, G., Wang, H., Liu, Y., ... & Yin, H. (2020). Elaboration of a multimodal MRI-based radiomics signature for the preoperative prediction of the histological subtype in patients with non-small-cell lung cancer. Biomedical engineering online, 19, 1-17. DOI

[35] Vale-Silva, L. A., & Rohr, K. (2021). Long-term cancer survival prediction using multimodal deep learning. Scientific Reports, 11(1), 13505. DOI

[36] Schulz, S., Woerl, A. C., Jungmann, F., Glasner, C., Stenzel, P., Strobl, S., ... & Foersch, S. (2021). Multimodal deep learning for prognosis prediction in renal cancer. Frontiers in oncology, 11, 788740. DOI